/

Article / Book Information

Title	Molecular dynamics study of one-component soft-core system: Thermodynamic properties in the supercooled liquid and glassy states
Authors	Junko Habasaki,Akira Ueda
Citation	J. Chem. Phys., Vol. 138, ,
Pub. date	2013, 3
URL	http://scitation.aip.org/content/aip/journal/jcp
Copyright	Copyright (c) 2013 American Institute of Physics

Molecular dynamics study of one-component soft-core system: Thermodynamic properties in the supercooled liquid and glassy states

Junko Habasaki and Akira Ueda
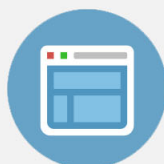
Molecular dynamics study of one-component soft-core system: Thermodynamic properties in the supercooled liquid and glassy states

Junko Habasaki[1] and Akira Ueda[2]

[1]*Department of Innovative and Engineered Materials, Interdisciplinary Graduate School of Science and Engineering, Tokyo Institute of Technology, Nagatsuta 4259, Yokohama 226-8502, Japan*
[2]*Department of Applied Mathematics and Physics, Faculty of Engineering, Kyoto University, Kyoto 606-8501, Japan*

Molecular dynamics simulations were performed to study the thermal properties of a supercooled liquid near the glass transition regime and of glasses in a one-component soft-core system with the pair potential $\varphi_n(r) = \varepsilon(\sigma/r)^n$, in which $n = 12$. The results are examined along a phase diagram, in which the compressibility factor defined by $\tilde{P}(\rho^*) \equiv PV/Nk_BT$ is plotted against the reduced density $\rho^* = \rho(\varepsilon/k_BT)^{3/n}$ (or the reduced temperature $T^* = \rho^{*-n/3}$). Similarly, a time-dependent dynamical compressibility factor can be plotted against the time-dependent reduced density $\rho_t^* = \rho(\varepsilon/k_BT_t^*)^{3/n}$ (or the reduced time-dependent temperature). Analytical expressions of the specific heats C_V and C_P and of the entropy, S, were obtained as a function of $\tilde{P}(\rho^*)$ or of the scaled potential U^*. Even for a rapid cooling process, the C_V values are found to be affected by non-equilibrium relaxations in the $\rho_0^* > 1.3$ region, where ρ_0^* is the given initial value of ρ_t^*. The problem of the Kauzmann paradox is discussed using these expressions. The fluctuation of the time-dependent temperature, T_t^*, which determines C_V, is characterized by the spectra that are obtained by multitaper methods. The thermal fluctuation along the non-equilibrium relaxation under *NVE* conditions was also examined. © *2013 American Institute of Physics*. [http://dx.doi.org/10.1063/1.4799880]

I. INTRODUCTION

The thermodynamics of super-cooled liquids and of their glass transition, such as rapid changes in the specific heat, has been an area of debate for a long time. One-component systems with the soft-core (SC) potential $\varphi_n(r) = \varepsilon(\sigma/r)^n$ [1–6] have been examined along a phase diagram using a compressibility factor, $\tilde{P}(\rho^*) \equiv PV/Nk_BT$, plotted against a reduced density, ρ^*, or a reduced temperature, T^*, using *NVE*-MD. (See Sec. II for the explanation of these terms.) In the present work, the specific heats of a one-component SC system were examined during both rapid cooling and non-equilibrium *NVE* relaxation processes to better understand the glass transition. The advantages of using a one-component system include not only the elimination of the mixing effects of different species but also the ability to rigorously treat the system using the phase diagram.

In the region, $\rho_0^* > 1.3$, where ρ_0^* is the given initial value of ρ_t^*, non-equilibrium relaxation (represented by Eqs. (6a) and (6b) in Sec. II) was observed.

Interestingly, using the time-dependent dynamic compressibility factor $(PV/Nk_BT)_t$ plotted against $\rho_t^* = \rho(\varepsilon/k_BT_t^*)$, non-equilibrium relaxation process toward the glass branch[1,5] can be also mapped on the same diagram.

Even during the rapid quenching of the system (the cooling rate is on the order of 1×10^{12} K/s for argon), a non-equilibrium relaxation starts in the region $\rho_0^* > 1.3$ and the system tends to be trapped midway along the relaxation path toward the glass branch on the diagram in the large ρ_0^* region.[5] Thus, in both the cases of rapid quenching and of a long run under an *NVE* condition, glassy states are obtained when

the dynamics are slow enough. The existence of these glassy states was determined using the dynamics and structures.[5] It is interesting to examine how the thermodynamic properties change along the different paths to the glassy state because the glass transition can be defined by the existence of a thermodynamic change in the system.

In the SC system, the specific heat C_V values of the liquid and of the super-cooled liquid were obtained as a function of $\tilde{P}(\rho^*)$ using a polynomial expansion of the $1/T^*$ terms, while the value of the quenched liquid state was treated as a function of the scaled potential energy, U^*, using an expansion of the T^* terms (see Sec. II). We also derived an expression for the entropy, S, using the coefficients of the polynomials mentioned above; the excess entropy of the system (the difference between that of the quenched liquid (glass) and of the crystal) was obtained in an analytical form. "Kauzmann's paradox,"[7] which is a long-standing problem in the field of glass transition, will also be discussed on this basis of the excess entropy. This topic may be considered misleading and confusing[8] for students in the field. Although we partially agree with this opinion, the concept still appears to be instructive and attractive for clarifying some of the problems of glass transition.

Furthermore, the fluctuation of the time-dependent reduced temperature, T_t^*, which controls the specific heat of the system, was examined using the spectra obtained by the multitaper method (MTM).[9–11]

II. THEORY

The behavior of the SC model is examined along the phase diagram, in which a compressibility factor defined by

$\tilde{P}(T^*) \equiv PV/Nk_BT$ (see Eq. (3)) is plotted against the reduced density ρ^* (or the reduced temperature, T^*). The fundamental relations among the thermodynamic quantities are summarized in Eqs. (1)–(7).[1,2,5]

The Hamiltonian of the SC system,

$$H(p,r) = \sum_i \frac{p_i^2}{2m} + \sum_{i<j} \varepsilon \left(\frac{\sigma}{r_{ij}}\right)^n \equiv K + U, \qquad (1)$$

can be rewritten as

$$H(p,r) = \varepsilon \left(\frac{\sigma}{l}\right)^n H^*(p^*, r^*), \qquad (2a)$$

$$H^*(p^*, r^*) = \sum_i \frac{p_i^{*2}}{2} + \sum_{i<j} \left(\frac{1}{r_{ij}^*}\right)^n. \qquad (2b)$$

Here, a unit system with length $l = (V/N)^{1/3}$, time $\tau = l(m/\varepsilon)^{1/2}(l/\sigma)^{n/2}$, and mass m was introduced. The values K^* and U^* are the scaled kinetic and potential energies, respectively.

According to the classical virial theorem combined with the NVE method, the compressibility factor, PV/Nk_BT, can be written as

$$\frac{PV}{Nk_BT} = 1 + \frac{n}{2}\frac{\langle U_t \rangle}{\langle K_t \rangle} = 1 + \frac{n}{3}\frac{\langle U_t^* \rangle}{NT^*} \equiv \tilde{P}(\rho^*), \qquad (3)$$

where the notation $\langle \cdots \rangle$ indicates the time average of the value in the brackets. $\tilde{P}(\rho^*)$ is given by a function of the reduced density (or the reduced temperature), which is defined by

$$\rho^* = \rho \left(\frac{\varepsilon}{k_BT}\right)^{3/n} = T^{*-3/n}, \qquad (4)$$

where $\rho = N\sigma^3/V$ is the non-dimensional number density.[5]

The dynamical compressibility factor $(PV/Nk_BT)_t$, which is defined by

$$\left(\frac{PV}{Nk_BT}\right)_t = 1 + \frac{n}{2}\frac{U_t}{K_t} \equiv g(\rho_t^*), \qquad (5)$$

is an important quantity, particularly when we consider the fluctuation of $g(\rho_t^*)$ that is caused by the energy transfer between the potential and kinetic energies.

$g(\rho_t^*)$ can be represented on the phase diagram as follows:[2,6]

$$g(\rho_t^*) = \left[g(\rho_0^*) + \left(\frac{n}{2} - 1\right)\right]\left(\frac{\rho_t^*}{\rho_0^*}\right)^{n/3} - \left(\frac{n}{2} - 1\right), \qquad (6a)$$

$$g(\rho_0^*) = \frac{n}{3}\frac{E}{\varepsilon N}\left(\frac{\rho_0^*}{\rho}\right)^{n/3} - \left(\frac{n}{2} - 1\right). \qquad (6b)$$

Here, $E = K_t + U_t$, $g(\rho_0^*)$ is the given initial value of $g(\rho_t^*)$ with a time-dependent reduced density that is defined by $\rho_t^* = \rho(\varepsilon/k_BT_t)^{3/n}$ and T_t is defined by $k_BT_t = 2K_t/3N$. The dynamical compressibility factor changes with time along the $g(\rho_t^*)$ curve, as represented by Eqs. (6a) and (6b); this change accompanies the fluctuation that is caused by the fluctuation of ρ_t^*. When ρ_t^* fluctuates within the region of a thermally equilibrated liquid state (or crystalline state), the long-time

averages $\langle \rho_t^* \rangle (\equiv \rho^*)$ and $\langle g(\rho_t^*) \rangle (\equiv \tilde{P}(\rho^*))$ provide the point of state on the diagram of $\tilde{P}(\rho^*)$ vs. ρ^*. If the initial point $(g(\rho_0^*), \rho_0^*)$ is located in the region of an unstable state, the system relaxes, fluctuating with ρ_t^*.

It is interesting to note that non-equilibrium relaxation under the constant pressure condition can be obtained in a similar manner, as will be shown in a separate paper; here, our attention is focused on NVE relaxation.

The pressure P is given by the following expression:[1,5]

$$P = \frac{\varepsilon}{\sigma^3}\left(\frac{k_BT}{\varepsilon}\right)^{3/n+1}\rho^*\tilde{P}(\rho^*). \qquad (7)$$

Using the compressibility factor, the specific heat of constant volume C_V is expressed as follows.

Introducing the non-dimensional quantity, $(E/Nk_BT) \equiv h(\rho^*)$, the internal energy is

$$\frac{E}{Nk_BT} = th(\rho^*), \qquad (8)$$

where $t = k_BT/\varepsilon$. C_V can then be obtained using

$$C_V = \frac{\partial}{\partial t}\left(\frac{E}{N\varepsilon}\right)_V = h(\rho^*) + t\frac{dh(\rho^*)}{d\rho^*}\left(\frac{\partial\rho^*}{\partial t}\right)_V$$

$$= h(\rho^*) - \left(\frac{3}{n}\right)^2\rho^*\frac{dh(\rho^*)}{d\rho^*}$$

$$= \frac{3}{2} + \frac{3}{n}[\tilde{P}(\rho^*) - 1] - \left(\frac{3}{n}\right)^2\rho^*\frac{d\tilde{P}(\rho^*)}{d\rho^*}$$

$$= \frac{3}{2} - \frac{3}{n} + \frac{3}{n}\tilde{P}(\rho^*) + \frac{3}{n}T^*\frac{d\tilde{P}(\rho^*)}{dT^*}, \qquad (9)$$

where we used the relation

$$h(\rho^*) = \frac{3}{2} + \frac{3}{n}[\tilde{P}(\rho^*) - 1]. \qquad (10)$$

In a similar manner, the specific heat of constant pressure C_P can be obtained by differentiating the enthalpy:

$$C_P = \frac{\partial}{\partial t}\left(\frac{E + PV}{N\varepsilon}\right)_P = j(\rho^*) + t\frac{dj(\rho^*)}{d\rho^*}\left(\frac{\partial\rho^*}{\partial t}\right)_P, \qquad (11)$$

where $((E + PV)/Nk_BT) \equiv j(\rho^*)$. Applying the condition of constant pressure, $d(P\sigma^3)/dt = 0$, to Eq. (7), we obtain

$$(1 + 3/n)\rho^*\tilde{P}(\rho^*) + t\frac{\partial}{\partial\rho^*}\{\rho^*\tilde{P}(\rho^*)\}\left(\frac{\partial\rho^*}{\partial t}\right)_P = 0. \qquad (12)$$

If we insert the $(\partial\rho^*/\partial t)_P$ that was obtained from Eq. (12) into Eq. (11), we obtain

$$C_P = j(\rho^*) - (1 + 3/n)\frac{dj(\rho^*)}{d\rho^*}\left[\frac{d}{d\rho^*}\ln\{\rho^*\tilde{P}(\rho^*)\}\right]^{-1}$$

$$= \frac{3}{2} - \frac{3}{n} + \left(\frac{3}{n} + 1\right)\tilde{P}(\rho^*) - \left(\frac{3}{n} + 1\right)^2\frac{d\tilde{P}(\rho^*)}{d\rho^*}$$

$$\times \left[\frac{d}{d\rho^*}\ln\{\rho^*\tilde{P}(\rho)\}\right]^{-1}, \qquad (13)$$

where

$$j(\rho^*) = \frac{3}{2} - \frac{3}{n} + \left(\frac{3}{n} + 1\right)\tilde{P}(\rho^*). \qquad (14)$$

From Eqs. (9) and (13), it can be determined that C_P is related to C_V by

$$C_P = C_V + \frac{\left[\left(\frac{n}{2}-1\right) - \frac{n}{3}C_V\right]^2}{\left(1+\frac{n}{3}\right)\tilde{P} + \frac{n}{3}\left(\frac{n}{2}-1\right) - \left(\frac{n}{3}\right)^2 C_V}. \quad (15)$$

To evaluate C_V numerically, the T^* dependence of $\tilde{P}(\rho^*)$ for the fluid state was determined using a high temperature expansion of $\tilde{P}(\rho^*)$, i.e., a polynomial of $1/T^*$:

$$\tilde{P}(\rho^*) = 1 + \frac{n}{3}\frac{\langle U_t^*\rangle}{NT^*}$$

$$= 1 + \frac{n}{3}\left\{\frac{B_1}{T^*} + \frac{B_2}{T^{*2}} + \cdots + \frac{B_k}{T^{*k}}\right\}. \quad (16)$$

The unknown coefficients $B_1, \ldots, B_k$ were determined in a manner similar to that in Ref. 6. Inserting Eq. (16) into Eq. (9), we obtain

$$C_V = \frac{3}{2} - \sum_{l=2}^{k}(l-1)\frac{B_l}{T^{*l}}. \quad (17)$$

The entropy is evaluated by integrating the thermodynamic formula, $C_V = T(\partial S/\partial T)_V$,

$$\frac{S(T^*)}{Nk_B} - \frac{S(T_{ref}^*)}{Nk_B} = \int_{T_{ref}^*}^{T^*}\frac{C_V}{T^*}dT^*. \quad (18)$$

Here, T_{ref}^* is the temperature of a reference state.

For a numerical calculation of the entropy, we used the difference $S(T_2^*) - S(T_1^*)$ for a fixed T_1^*:

$$\frac{S(T_2^*)}{Nk_B} - \frac{S(T_1^*)}{Nk_B} = \frac{3}{2}\ln\left(\frac{T_2^*}{T_1^*}\right) + \sum_{l=2}^{k}(l-1)/l\left(\frac{B_l}{T_2^{*l}} - \frac{B_l}{T_1^{*l}}\right). \quad (19)$$

In the present work, a reference value T_1^* in the high T^* region is commonly used for a liquid, supercooled liquid, quenched glass, or fcc crystal. Thus, the entropy is given by values relative to $S(T_1^*)/Nk_B$ for a fixed temperature T_1^*.

The value at the freezing point is $S(T_f^*)/Nk_B - S(T_1^*)/Nk_B$.

The entropy $S(T_m^*)$ at the melting point T_m^* is determined by the fluid-crystal coexistence condition, i.e., the condition that the Gibbs energy $G(t,\rho)$ and the pressure $P(t,\rho)$ at the melting point are equal to those at the freezing point:

$$\frac{S(T_m^*)}{Nk_B} = \frac{1}{Nk_B T}[E + PV - G]_m$$

$$= h(T_m^*) + \tilde{P}(T_m^*) - \frac{1}{Nk_B T}G(t, \rho_f), \quad (20)$$

where the Gibbs energy $G(t, \rho_m)$ is replaced by $G(t, \rho_f)$. The freezing entropy $\Delta S(T_{f\text{-}m}^*)$ is given by

$$\frac{\Delta S_{f-m}}{Nk_B} \equiv \frac{S(T_m^*)}{Nk_B} - \frac{S(T_f^*)}{Nk_B}. \quad (21)$$

For a numerical evaluation, we used the following values for the melting and freezing conditions, which were obtained by Ogura et al.:[12]

$$\rho_f^* = 1.173 \quad \text{and} \quad \rho_m^* = 1.217.$$

The entropy of the crystalline state at T^* is

$$\frac{S(T^*)}{Nk_B} = \frac{\Delta S_{m-f}}{Nk_B} + \frac{S(T_f^*)}{Nk_B} + \int_{T_m^*}^{T^*}\frac{C_V}{T^*}dT^*. \quad (22)$$

The numerical evaluation of the third term was performed in a manner similar to that in Ref. 6.

We approximate $\langle U_t^*\rangle$ by the kth polynomial of T^*, first applying the Chebyshev polynomials $\{T_n(T^*)\}$, $n = 1,2,\ldots,k$ and then rearranging them to obtain

$$\langle U_t^*\rangle = U_0^* + N(C_1 T^* + C_2 T^{*2} + \cdots + C_k T^{*k}). \quad (23)$$

The $(k+1)$ unknown constants $U_0^*, C_1, C_2, \ldots, C_k$ are determined from the least square fitting of $\langle U_t^*\rangle$. When Eq. (23) is inserted into Eq. (3), the compressibility factor becomes

$$\tilde{P}(\rho^*) = 1 + \frac{n}{3}\frac{U_0^*}{NT^*} + \frac{n}{3}\{C_1 + C_2 T^* + C_3 T^{*2}$$

$$+ \cdots + C_k T^{*k-1}\}. \quad (24)$$

By inserting Eq. (24) into Eq. (9), we obtain

$$C_V = \frac{3}{2} + C_1 + 2C_2 T^* + 3C_3 T^{*2} + \cdots + kC_k T^{*k-1}. \quad (25)$$

The entropy is again evaluated using Eq. (18) and we obtain

$$\frac{S(T^*)}{Nk_B} = \frac{\Delta S_{f-m}}{Nk_B} + \frac{S(T_f^*)}{Nk_B} + \left(\frac{3}{2} + C_1\right)\ln\left(\frac{T^*}{T_m^*}\right)$$

$$+ \sum_{l=2}^{k}\left(\frac{l}{l-1}\right)C_l[T^{*l-1} - T_m^{*l-1}]. \quad (26)$$

The entropy is represented by Eq. (19) for $T_f^* < T^* < T_1^*$ and by Eq. (26) for $0 < T^* < T_m^*$.

In the present work, Eq. (19) was used for the extended region $T_p^* < T^* < T_1^*$ which includes the supercooled liquid state, while the entropy values for the rapidly quenched system $0 < T^* < T_p^*$ were obtained using a manner similar to that for the crystal. Here, T_p^* ($\sim$0.31) is the temperature at which the specific heat C_V has a peak (see Fig. 3). The numerical value of T_p^* was obtained from the intersection of the C_V curves, which is expressed by Eq. (17) for the larger T^* region and by Eq. (25) for the smaller T^* region.

The ideal gas state may be used as a reference state for a high-temperature expansion. The absolute value of the entropy of an ideal gas is given by[13]

$$\frac{S^{id}}{Nk_B} = \ln\left[\left(\frac{2\pi mk_B T}{h^2}\right)^{3/2}\frac{Ve^{5/2}}{N}\right], \quad (27)$$

which can be rewritten as

$$\frac{S^{id}(T^*)}{Nk_B} = \frac{3}{2}\ln\left(\frac{2\pi T^*}{h^{*2}}\right) + \frac{5}{2}, \quad (28)$$

where h^* is the scaled Planck constant defined by $h = h^* ml^2/\tau$. Inserting Eq. (28) into Eq. (19), we obtain the

entropy at temperature T^*:

$$\frac{S(T^*)}{Nk_B} = \frac{3}{2}\ln\left(\frac{2\pi T_{ref}^*}{h^{*2}}\right) + \frac{5}{2} + \frac{3}{2}\ln\left(\frac{T^*}{T_{ref}^*}\right)$$
$$+ \sum_{l=2}^{k}(l-1)/l\left(\frac{B_l}{T^{*l}} - \frac{B_l}{T_{ref}^{*l}}\right). \qquad (29)$$

With increasing temperature toward T_{ref}^*, the entropy converges to that of an ideal gas.

Interestingly, the numerical value of the ideal gas depends on the scaled Planck constant (therefore, it is not constant) and depends on the ml^2/τ of the system. The difference in the entropies at temperatures T_1^* and T_2^* derived by Eq. (29) agrees with that given by Eq. (19).

The methods that were based on the equilibrium thermodynamics may not be suitable for examining the thermodynamics near the glass transition because of the non-equilibrium and/or non-ergodic nature of this transition.[8] The values C_V and S of this region are the time-averaged ones and not the ensemble-averaged ones. The time-dependent C_V values, which are based on the fluctuation of T^*, are also examined, as will be shown in Subsection IV F.

III. MOLECULAR DYNAMICS SIMULATIONS

Here, we study the behavior of a soft-core system with a pair potential, $\phi_n(r) = \varepsilon(\sigma/r)^n$ ($n = 12$), using molecular dynamics (MD) simulations with our MD program. Systems with 2048 particles and periodic boundary conditions were used for the simulations of liquids and glasses. The MD simulations were performed using argon-like parameters, although reduced units are used unless otherwise stated.

In the present work, the thermodynamics during a rapid cooling process by the scaling of the velocity (run 1, cooling rate of $\sim 1 \times 10^{12}$ K/s for argon) was examined.

Some runs along *NVE* relaxations (see Sec. IV A for the outline and Ref. 5 for details) were also examined. The results are compared with the thermodynamics along the crystal branch that was examined in a previous work.[6] The time step was either 1 or 4 fs (for argon).

Additionally, the heating process by the scaling of the velocity (run 2, heating rate of $\sim 1 \times 10^{11}$ K/s) starting from the quenched state at ~ 0 K was examined.

IV. RESULTS AND DISCUSSION

A. Phase diagram and classification of the glasses

Before mentioning the thermodynamics results of the SC system along the phase diagram, the characteristics of the diagram, which was previously examined,[1,5] are summarized here. Hereafter, the compressibility factor $\tilde{P}(\rho^*)$ is represented by g^* and the time-dependent dynamical compressibility factor is denoted by g_t^*. Both compressibility factors are represented by g^* in the diagram.

In Fig. 1(a), the diagram that includes the metastable glass branch is shown for the system with 2048 particles. The system along the liquid (and supercooled liquid) branch is un-
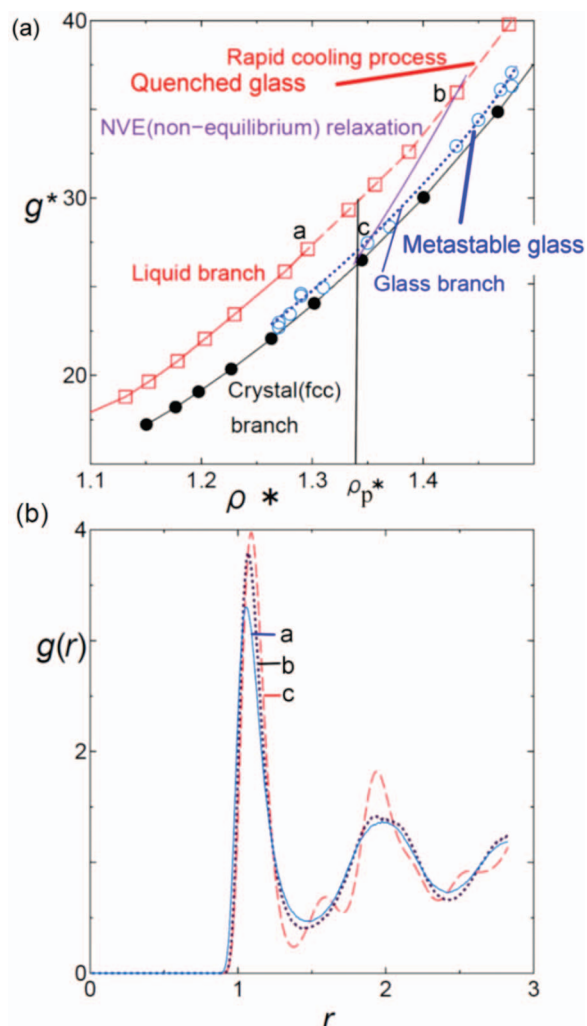

FIG. 1. (a) Phase diagram of the soft-core system. Data for the liquid (and quenched glass) branch (red open squares) and for the crystal (fcc) branch (black filled circles) are shown. The blue circles are the points for the metastable states that were obtained in our previous work[5] after *NVE* relaxations. The dotted blue curve shows the glass branch that represents these points. The position of ρ_p^* ($= T_p^{*-0.25}$) is also shown in the diagram. The data points obtained from rapid cooling (run 1) are connected by the dashed red curve. An example of the trajectory of g_t^* for *NVE* relaxation is shown by the solid purple curve on the diagram. (b) Pair correlation functions, g(r), for several points ((a), (b), and (c), shown in (a)) on the phase diagram.

stable for $\rho_0^* > 1.3$ and initiates a non-equilibrium relaxation process toward the glass or crystal branch with/without some leading times. The position ρ_p^* ($= T_p^{*-0.25}$) is also shown in the diagram.

Many systems were found to reach metastable states before the crystal branch was attained. (For example, the system at the glass branch was confirmed to be nearly stable even after 37 ns (for argon) for the case starting from $\rho_0^* = 1.357$). By connecting the metastable states in the phase diagram, we obtain the glass branch where the dynamics of the particles are almost frozen. Therefore, we call the systems in these metastable states "metastable glasses."

Non-equilibrium relaxation from the liquids-supercooled liquids branch to the glass branch can be regarded as the glass transition.
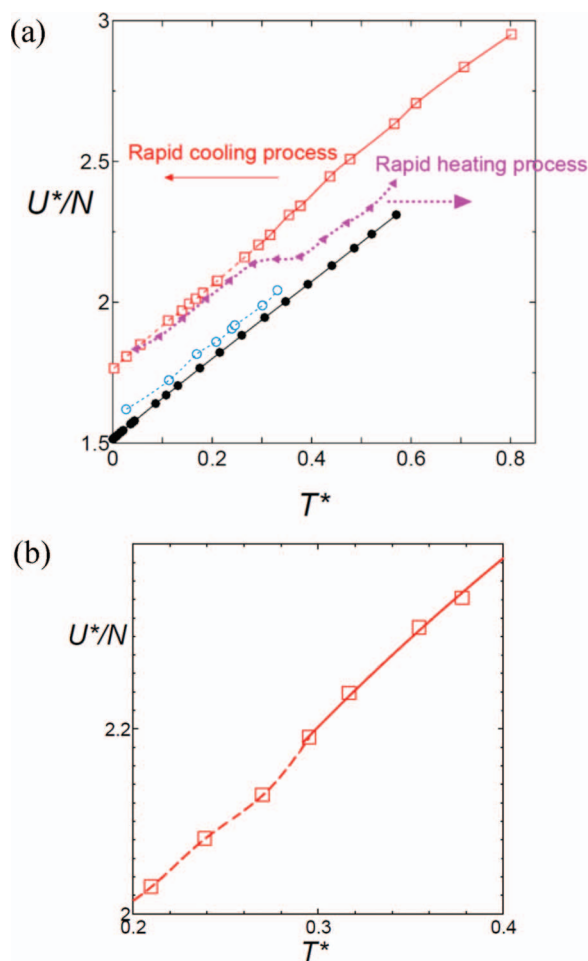
FIG. 2. (a) U^*/N values for rapid cooling along the liquid branch (red open squares) that is shown in the phase diagram in Fig. 1. The values for the glass branch (blue circles) and for the crystal (fcc) branch (black filled circles) are also shown. The values for the rapid heating process (pink filled triangles) are also plotted. (b) The plot on an enlarged scale for the rapid cooling case shown in (a).

TABLE I. The values g^* that are used for the calculation of C_V along the rapid cooling of the system (run 1). U^*/N values are also shown for the low T^* region. The values for $\rho^* < 1.3$ are for the equilibrated states. The values for $\rho^* \sim 1.36$ are for the quasi-equilibrated state before non-equilibrium relaxation. The values for $\rho^* > \sim 1.4$ are for the trapped states.

ρ^*	T^*	$1/T^*$	g^*	U^*/N
2.447	0.0279	35.88	254.63	1.76355
2.042	0.0575	17.39	128.27	1.80410
1.726	0.1128	8.867	67.994	1.88532
1.635	0.1400	7.1408	56.026	1.92252
1.595	0.1544	6.4767	51.426	1.94245
1.563	0.1677	5.9625	48.063	1.96940
1.529	0.1828	5.4713	44.685	1.99203
1.478	0.2097	4.7677	39.781	2.02931
1.431	0.2388	4.1875	35.937	2.08158
1.387	0.2700	3.70	32.596	2.12861
1.371	0.2828	3.536	31.305	2.13799
1.357	0.2952	3.387	30.748	2.19115
1.333	0.3167	3.157	29.322	2.23885
1.296	0.3545	2.821	27.118	2.30971
1.275	0.3778	2.647	25.844	2.34195
1.230	0.4370	2.289	23.432	2.44634
1.203	0.4772	2.096	22.056	2.50789
1.179	0.5181	1.930	20.800	2.57462
1.1527	0.5664	1.766	19.638	2.63361
1.132	0.6098	1.640	18.788	2.70620
1.107	0.6653	1.503	17.724	2.83549
1.083	0.7267	1.376	16.756	…
1.063	0.7827	1.278	15.998	…
1.045	0.8376	1.194	15.327	…
1.031	0.8846	1.130	14.825	…
1.015	0.9406	1.063	14.295	…
0.948	1.2375	0.8081	12.150	…
0.891	1.5847	0.6311	10.577	…

In the case of rapid cooling, a transition to the non-equilibrated state occurs in the larger ρ_0^* region ($\rho_0^* > 1.36$) and tends to be trapped midway along the path to the glass branch at larger ρ^*.[5] When the dynamics in the trapped states are slow enough, these states can also be regarded as glassy states. We term these states "quenched glasses." In such cases, slow relaxations toward the glass branch, i.e., an "aging processes," will follow over a longer time scale.

The pair correlation functions, g(r), are shown in Fig. 1(b) for the systems located at positions a, b, and c on the diagram in Fig. 1(a). Point a is for the liquid state, point b is for the quenched liquid and point c is located on the glass branch. The structures in the rapidly quenched systems are liquid-like, and a splitting in the second peak of g(r) is observed. This structure is almost unchanged with an increase in ρ^*, except for the heights of the peaks in g(r). The g(r) of point c on the glass branch includes the peaks that correspond to both the bcc and fcc structures, which form the inverse lattice of each other, and has no crystalline peaks on a longer length scale. The data indicate that the system on the glass branch is a complicated mixture of substructures of both forms on

the atomistic level and is not mixed nano-crystals, although some overlap of the crystallization process was found in several cases. (See Ref. 5 for details.)

In Fig. 2(a), the T^* dependence of the U^* values for the same rapid cooling run (see Table I) and for a rapid heating run is shown. Figure 2(b) shows the dependence on an enlarged scale. The corresponding changes in the C_V and C_p values are shown in Fig. 3. A change in the slopes of g^* or U^* was found at $T^* \sim 0.31$. This temperature corresponds to the T_p^* (the peak position of the specific heats) that was mentioned in Sec. II.

The determination of the coefficients of the polynomials, C_1 for $T_p^* > 0.31$ and B_1 for $T_p^* < 0.31$, will be shown in Secs. IV B and IV C, respectively.

In the rapid cooling case, T^* characterizes the beginning of the solid-like states and C_V, which is ~ 3 ($T^* \sim 0.10$), is defined as T_g^*, below which the C_V curves of the super-cooled liquid and crystalline states almost coincide with each other, as shown in Fig. 3(a).

Several definitions of T_g have been used in literatures. The usual thermodynamic T_g appears to be located between the two temperatures T_g^* and T_P^*, that are defined in the present work.
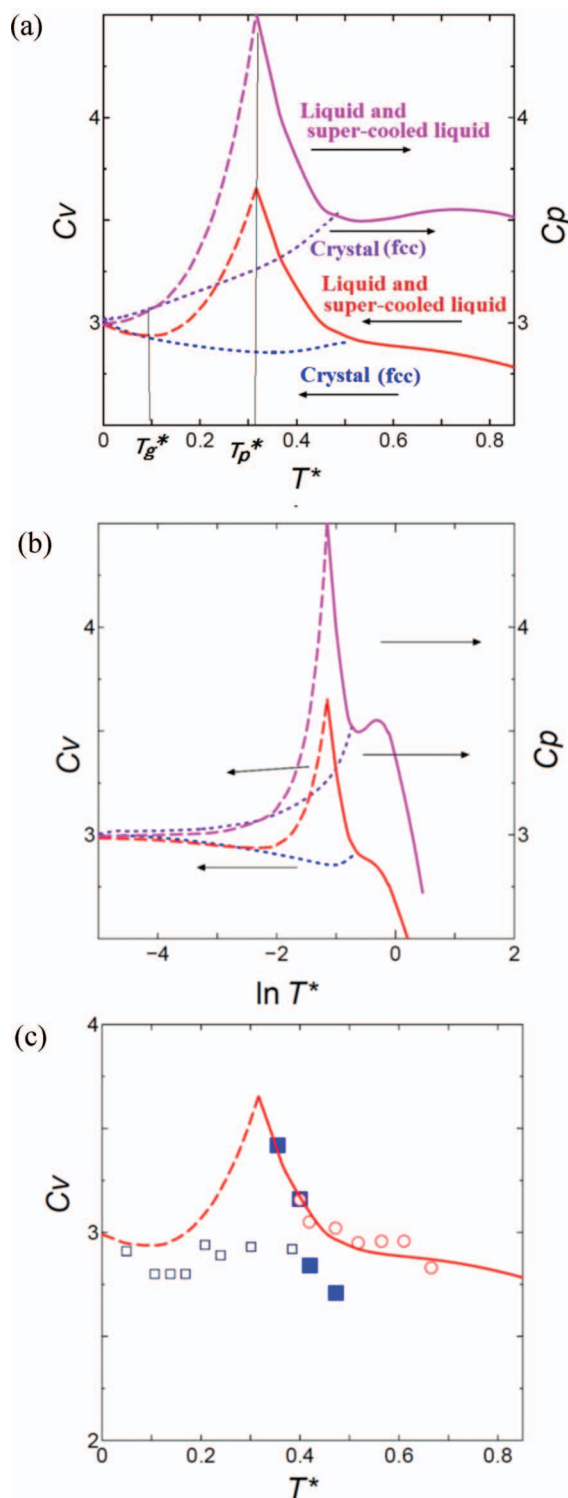
FIG. 3. (a) The C_V curves along the rapid quenching (run 1), obtained from polynomial fitting using Eqs. (16) and (17) for $T_P^* < T^*$ (red solid curve) ($T_P^* \sim 0.31$) and using Eqs. (23) and (25) for $T^* < T_P^*$ (red dashed curve). The C_P values for $T_P^* < T^*$ (pink solid curve) and for $T^* < T_P^*$ (pink dashed curve) calculated from Eq. (15) are also shown. The C_V values (blue dotted curve) and C_P values (purple dotted curve) for the crystalline states (fcc) (Ref. 6) are shown for comparison. (b) Similar plots as in (a) versus $\ln T^*$. (c) C_V obtained from the fluctuation of the kinetic energy using Eq. (30) along the rapid quenching of a liquid. Red circles: the C_V values obtained using an averaging time of 100 ps (for argon) in the liquid state. Blue filled squares: the C_V values obtained using an averaging time of 20 ps (for argon) before *NVE* relaxation. The values for the short time scale change more rapidly. Black squares: The values along the glass branch, in which an averaging time longer than 1 ns was used.

TABLE II. Coefficients, B_n, obtained for the liquid and rapidly quenched liquid states using Eq. (16). The C_V values were calculated for $T^* > 0.33$ using these coefficients. The relation between the observed g^* values and the ones calculated using the coefficients is shown in the last row with the goodness of fit for the region $0.33 < T^* < 1.58$.

Coefficients of the power law expansion	(by Chebyshev polynomials using T_0-T_6 terms) (Data in the region $0.26 < T^* < 1.58$ were used)
B1	5.6200
B2	-4.1928
B3	2.42566
B4	-0.75967
B5	0.120673
B6	-0.0076763
	y = 0.999x + 0.015, R^2 = 1.000

B. Polynomial fitting of g* for the liquid branch

In Table I, the g^* values that were examined for the liquid branch and along the rapid quench of this branch (run 1) are shown. In the equilibrium states, these values are taken from the average of more than 100 000 steps (1 step = 1 fs for argon) (in the region $T_P^* < T^*$). The U^* values in the low T^* region are also shown and are used to obtain the coefficients of the polynomials in Eq. (23).

In Table II, the coefficients B_n of the expansion that was obtained along the liquid branch are listed. Non-equilibrium relaxation occurs after some leading times for $T^* \approx T_P^*$. For these T^*, g^* values were taken from the 20 000-step run that was performed before relaxation.

C. Polynomial fitting of U* for the rapidly quenched liquid

For the rapidly cooled liquid (run 1), the coefficients C_n of the low temperature form expansion (Eq. (23)) were obtained using a 4th order Chebyshev polynomial.

In Table III, the results are listed with those of the fcc crystal obtained in a previous work.[6] At temperatures less than T_P^*, the onset of non-equilibrium relaxation was inevitable; therefore, a 20 000-step run during the initial stages of relaxation was used for the polynomial fitting. In this case, C_0 is the value for the small T^* (large ρ^*) limit. The coefficient C_1 (= 1.49) in Table III is similar to that of the crystal (1.5), as expected for solid-like states. The value $C_1 \sim 3/2$ in the rapidly quenched glass in the present work suggests that the system behaves like harmonic oscillators in cages near 0 K. The 2nd and higher terms correspond to the anharmonic motions of the particles. At $T = 0$ K, the thermal energy becomes 0, and the term $3/2k_BT$ will disappear.

In the rapidly cooling run shown in Fig. 1, a change in the slope of g^* was observed at $T^* \sim T_P^*$.

This deviation from the ideal curve of the liquid branch is caused by non-equilibrium relaxation. As shown in Figs. 2(a) and 2(b), a clearer change in the slope at approximately $T^* \sim T_P^*$ can be found in the plot of U^*/N versus T^*. A nearly constant slope is observed in the region

TABLE III. Results of the C_n coefficients for rapidly quenched liquids, including the non-equilibrium and trapped states (run 1). The C_V values were obtained from these coefficients using Eq. (25). The relation between the observed U^*/N values and the ones calculated using the coefficients is shown in the last row with the goodness of fit for the region $0.0017 < T^* < 0.38$.

Coefficients of power law expansion	(by Chebyshev polynomials using T_0-T_4 terms) $0.0017 < T^* < 0.3778$	(by Chebyshev polynomials using T_0-T_6 terms) for fcc crystal
$C_0+U_0^*/N$	1.7212	1.5128
C_1	1.4911	1.5212
C_2	-0.50015	-0.91027
C_3	0.65508	4.4804
C_4	6.1907	-14.848
C_5	...	24.802
C_6	...	-15.450
	y = 0.9986x + 0.0029, R^2 = 0.999	y = 0.9935x − 0.0003, R^2 = 1.000

$T^* < 0.1 (\approx T_g^*) \sim 0.2$, and the system is considered to be in a trapped state. The U^*/N data along the glass branch (pale blue circles) and the fcc crystal branch (black circles) are also shown in Fig. 2(a).

D. Non-equilibrium character of the rapidly quenched system

In the case of *NVE* conditions, the non-equilibrium character can be easily detected by changes in the T^* during the runs[1,5] as well as by changes in U^* and g^*.

The non-equilibrium character can also be detected by the irreversibility of the process, even for the case of rapid quenching.

As shown in Fig. 2(a), the U^* values of the heating process of the system (after quenching at 0 K) were examined using the heating rate $\sim 1 \times 10^{11}$ K/s. The heating curve has a flat region at approximately $T^* \sim 0.3$. The difference between the cooling and heating curves becomes clear at approximately $T^* = 0.25$, and this difference becomes larger at $T^* = 0.3$-0.4. In this case, the U^* values did not reach those of the liquid branch, even at $T^* = 0.56 (>T_m^*)$, at least for the 50 000-step run. This trend is explained as follows. In the region $0.25 < T^* < 0.4$, relaxation toward the glass/crystal branch occurred during the heating process in a manner similar to that during the cooling process because of the exothermic character of the process, and this relaxation competed with the changes toward the liquid branch.

The details of the behavior of the systems during the cooling process and the irreversible part of the thermodynamics in the $T^* < T_P^*$ region change on a case by case basis because they are sensitive to the cooling or heating schedule and because the relaxation has several stages (see Fig. 6 and Ref. 5) that appear intermittently. Irreversibility is evidence of non-equilibrated relaxation in this T^* region.

The existence of a hysteresis in the glass transition during the cooling and heating cycles indicates that a memory of the thermal treatment procedure remains in the system. As shown in our previous work,[5] the structural changes in the *NVE* relaxation develop from a short length scale to the longer length scales of the structures. It is possible that the length scale of

the region that is affected by changing T^* during the cooling process is not the same as that affected during the heating processes, although further details of this phenomenon are beyond the scope of this work. In the medium ρ_0^* region, the time scale of non-equilibrium relaxation is comparable to that of the diffusion process. Therefore, g^* and U^* are significantly affected by the non-equilibrium character of the process.

Accompanied by changes in the slopes of g^* and U^*, the derivative of g^* in Eq. (9) changes twice: when the system is drawn to non-equilibrium relaxation and when the system is trapped in a localized state. The former change corresponds to T_P^*, while the latter corresponds to T_g^*, i.e., the C_V values obtained from Eq. (9) are not continuous at both T_P^* and T_g^*.

If the values for each T^* are observed using narrow time and T^* windows, the behavior looks discontinuous. On the other hand, the behavior that is usually observed in experiments looks continuous.

E. C_V and C_P values obtained from the coefficients of the rapidly quenched system

In Fig. 3(a), the C_V values that were obtained for the liquid and rapidly quenched liquid (run 1) states are shown by the red solid curve and by the red dashed curve, respectively. For comparison, the C_V values that were obtained for the crystal (fcc) branch are shown by the blue dotted curve.

The C_V values of the rapidly cooled system exhibit a maximum at T_P^* and decrease with decreasing T^*.

The C_P values for the liquid and rapidly cooled liquid (pink solid curve and dashed curve) that were calculated using Eq. (15) are also shown, as are those for the fcc crystal (purple dotted curve).

The changes in the slope of C_V or C_P are accompanied by the derivative of g^* or U^*. Thus, a rapid change in C_V or C_P is accompanied by the beginning of non-equilibrium relaxation and the trapping that follows it. Both C_V and C_P decrease with decreasing T^* below T_P^*, and they become comparable to those for crystals at T_g, i.e., $T^* = 0.14$ ($\rho^* = 1.63$, $\ln(T^*) = -2.0$). Similar coincidences between the C_P values were previously found for the zero pressure isobar of a quenched Lennard-Jones system and for the crystal of this

system at $\ln(T/K) \sim 3.5$ ($T/T_f \sim 0.42$).[14] Both the C_V and C_P values appear to converge to the limiting value of $C_V \sim 3.0$ at 0 K, which is the typical value for the classical solid state.

Our results for C_P qualitatively coincide with those of Cape and Woodcock[14] (see Fig. 2 (the C_P vs. $\ln(T)$ plot) in Ref. 15), in which the C_P values were obtained from an expansion as a function of ρ^*. Similar results for the changes in C_P near the glass transition region have been obtained using experiments[16] and simulations[17] for ionic liquids.

F. C_V values obtained from the fluctuation of the temperature

Mauro et al.[18] pointed out that, for a non-equilibrium or non-ergodic material, the equations from equilibrium thermodynamics are not directly applicable to the glassy state without additional information on the details of the microscopic fluctuations. Thus, the question arises whether a method similar to that for the equilibrated system is applicable to the present system or not. In this section, we examine the thermodynamics based on the fluctuation.

We used the following expression for the specific heat, C_V, which is based on the fluctuation in the micro-canonical ensemble that was derived by Lebowitz et al.,[19]

$$C_V = \frac{d/2}{1 - (Nd/2)(\langle K^2 \rangle - \langle K \rangle^2)/\langle K \rangle^2}, \quad (30)$$

where d is the dimensionality of the system. The ensemble average $\langle K \rangle$ is replaced by the time average of the K_t values, in which the fluctuation occurs along the $g(\rho_t^*)$ curve. In the case of the micro-canonical ensemble, the variance of K is equal to that of U.

The C_V values that were obtained from the fluctuation of the system on the liquid branch (red circles) are shown in Fig. 3(c). The C_V values are also the time-averaged and not the ensemble-averaged ones. Near T_p^*, a short time scale (20 ps for argon) was used to obtain U^* or g^* to avoid the large contribution of non-equilibrium relaxation. Therefore, the C_V values that were obtained within this time scale (blue filled squares) were also plotted. The short time values appear to change more rapidly than those from the longer time scale, although the numerical errors are larger for the former.

In the region $T^* < T_P^*$, the C_V values obtained from the fluctuation are unstable because of the contribution of non-equilibrium relaxation. The values during relaxation are sensitive to the time scale of the observation, as shown later.

The calculation of C_V using the fluctuation is also applicable to the systems on the glass branch. The black squares in Fig. 3(c) are the values on the glass branch (the metastable state after NVE relaxations) and were obtained using Eq. (30). For this branch, we used a run that was longer than 1 ns (for argon) for each point to obtain a nearly stable point. The values tend to spread around 2.8–3.0. When we increased the temperature, starting from the smallest T^* on the glass branch, slightly larger values (3.0–3.3 at $T^* = 0.1$–0.35 for 6 points) were obtained (not shown).

As shown in Fig. 3(c), the C_V values that were obtained from the derivatives of the energy and those from the fluctu-

ations of the kinetic energy are comparable if the averaging time is comparable. This result is natural because the U^* and g^* values are obtained from the quasi-equilibrated states during the same runs. Thus, the equation for C_V that was derived for the time-averaged energy is applicable as long as g^* or U^* can be represented by polynomials.

G. Non-equilibrium and non-ergodic character of the system

The origin of the time dependent behavior of C_V near the glass transition is controversial. Carruzzo and Yu,[20] who examined a three-dimensional binary mixture of soft-core systems in NVT ensembles, argued that the system falls out of equilibrium and becomes trapped in a basin in the energy landscape below $T < T_P$. However, Yu and Carruzzo[21] later suggested that the specific heat peak is the result of not sampling enough of the phase space at $T < T_P$. The author observed that, just below T_P, the system is equilibrated in the sense of showing no signs of aging. They observed that the C_V values that were calculated from the energy fluctuation and from the derivative of the energy coincided when parallel tempering, in which the distribution is forced to be Boltzmann type, was used. In Ref. 20, a time-dependent behavior was observed for $t_W < 10^6$ MD steps. This behavior may be explained based on our observation of non-equilibrium relaxation, i.e., the relaxation process contributes before this time and the system reaches the glass branch after $t_W > 10^6$.

Horrowell's group[22, 23] argued that the specific heat peak in two-dimensional binary SC mixtures is an equilibrium feature that arises due to fluctuations between different local minima.

Tao et al.[24] calculated the specific heat based on the free-energy landscape. The authors explained that the abrupt changes in C_V are due to changes between the annealed and quenched states. In their work, the glassy state is regarded as a state that cannot relax to an equilibrium state within the observation time. The time scale of the observation and the probability of residence in the basins play important roles in this situation.

Some of the inconsistencies of these works that are related to the equilibrium and non-equilibrium character of the behaviors will be eradicated when the positions of the system on the phase diagram are taken into account. Due to the slow dynamics near the glass transition, the non-equilibrium states and non-ergodicity might be difficult to distinguish from each other. Some of the other inconsistencies may arise from the fact that both insufficient sampling times for the slow dynamics and non-equilibrium relaxation may result in a similar time-dependent behavior of C_V.

In our observations, the system is regarded as non-ergodic for $T^* < T_P^*$ because the observation time is shorter than the relaxation time of the system, and this feature is combined with non-equilibrium relaxation toward the different states. The latter is related to the pathway in the phase space of the glass transition. We also found that the non-ergodic character is related to the trapping of the trajectory in the phase-space, and a similar situation was reported for the crystalline state in the low T^* region.[6]

H. Excess entropy and Kauzmann's paradox

Kauzmann[7] suggested that the entropy of a liquid decreases rapidly upon cooling toward the glass transition temperature and can be extrapolated to unreasonable values at lower temperature contradicting the third law of thermodynamics, which posits that the entropy of a liquid cannot be less than the entropy of a crystal. This paradox has been discussed many times in regard to glass transition problems, and many answers for this problem have been proposed.[7,25–29] In the original paper by Kauzmann, the energy barrier to crystallization was assumed to be on the same order as the thermal energy, and crystallization was therefore considered unavoidable.

One of the probable answers is that the extrapolation is not allowed because the status of the liquid changes to the glassy state before T_K is attained. The temperature T_K is regarded as the ideal glass transition point[26] or as a lower limit to the glass transition temperature of the system, at which the "ground state" of disordered packing is attained.[27]

Stillinger[28] argued that further relaxation among the different microstates results in a change in the configurational entropy toward zero at 0 K and that there is, therefore, no conflict with the third laws. Speedy[29] showed, using simulations of hard core models, that, regardless of how the liquid entropy is extrapolated, the Kauzmann temperature cannot be reached because the entropy of the glasses with the same enthalpy as the liquid is greater than that of the crystal. A similar situation has been observed in experiments.[15]

Additional effects that are related to the time scale of the observation overlap this phenomenon. Near T_g, the α-relaxation of the system becomes so slow that the liquid can no longer equilibrate within the observation time. Therefore, the slowing down of the dynamics near the glass transition will affect the observed changes in the entropy, especially within the limited time scale of MD simulations. Thus, many problems that are concerned with the paradox appear to be explained by considering the situation near the ideal glass or at a slower relaxation time than the observation time. However, some of the problems are not adequately solved. For example, Kivelson and Tarjus[25] argued that the rather rapid changes in S_{liq} near the glass transition appear to be difficult to explain using the observation time scale.

In the present work, we will distinguish two cases, toward the quenched glass and toward the metastable glass, for the arguments of the Kauzmann paradox.

I. Changes in the entropy during the rapid cooling

In Fig. 4(a), the entropies, S, of the liquid (and supercooled liquid) ($T^* > T_P^*$, red solid curve) and of the crystalline states (blue curve) are shown. The former and latter curves are obtained using Eqs. (19) and (26), respectively. A curve for the rapidly cooled system ($T^* < T_P^*$, red dashed curve) is connected to the red solid curve at T_P^*, at which the behavior changes significantly. The $|\Delta S_{f\text{-}m}|/Nk_B$ value for melting was determined to be 0.975.

The slope of the S versus T^* (or $\ln T^*$) plot for the rapidly cooled system is larger than that for the crystal near T_P^*. This
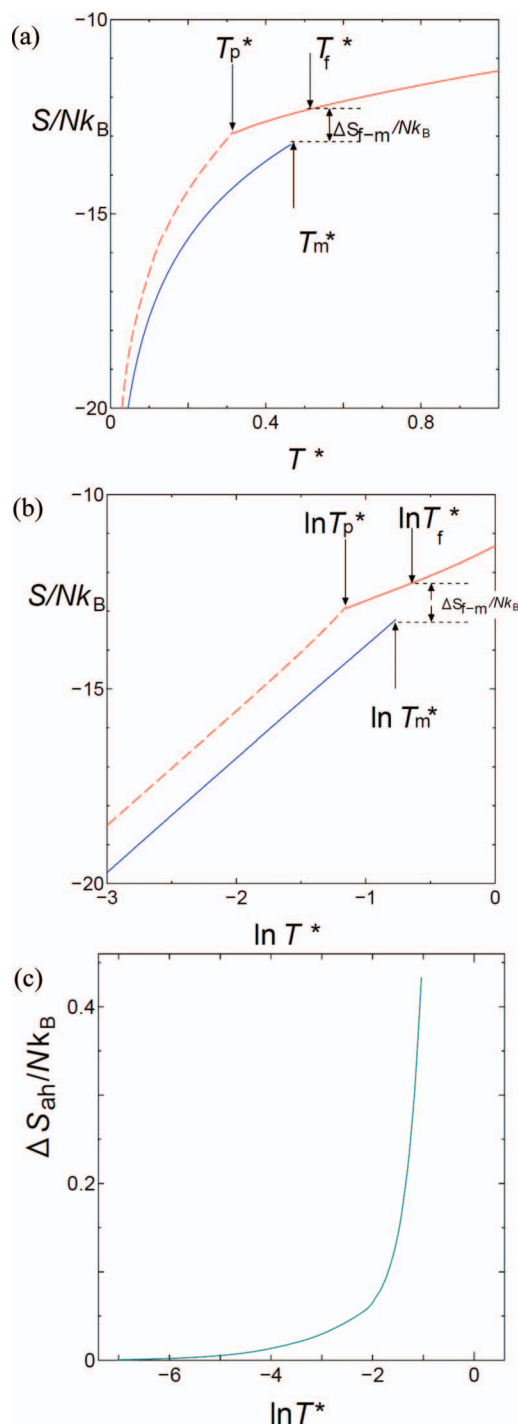

FIG. 4. (a) Entropy curves obtained along the rapid quenching liquid (glass) plotted against T^*. The same color as in Fig. 3(a) is used. (b) Entropy curves obtained along the rapid quenching liquid (glass) plotted against $\ln T^*$. (c) The anharmonic contribution of the excess entropy, ΔS_{ah}, obtained using Eq. (31) (green solid curve). The logarithmic term was omitted because C_{1ql} (the C_1 value for the quenched liquid (glass)) is comparable to C_{1cryst} (the C_1 value for the fcc crystal). The contribution of the residual entropy was also omitted. The ΔS_{ah} value appears to converge to 0 in the $T^* \sim 0$ limit.

slope decreases toward 0 K with some residual entropy; therefore, the paradox does not occur, although the extrapolated curve of this region and the crystalline curve may meet at the Kauzmann temperature.

In the low T^* region, the contribution of the logarithmic term is comparable to that for the crystal because of the similar C_1 values, shown in Table III. This result is consistent with the fact that the slope of the U^*/N versus T^* plot of the rapidly quenched system is similar to that of the crystalline state in the low T^* region.

As shown in Figs. 4(a) and 4(b), the difference in the entropy of liquid and crystal including the fusion entropy slightly decreases in the region where the non-equilibrium relaxation contributed but did not smear out at $T^* = 0$. This situation is similar to that observed for hard sphere glass.[30]

The difference in the entropy (the excess entropy), ΔS, of the quenched liquid (glass) and the crystal can be directly obtained from the following expression if the common reference T^* in a sufficiently low temperature region is used.

The residual entropy at $T^* = 0$ that can be observed in Figs. 4(a) and 4(b) is neglected here:

$$\frac{S_{ql}(T^*)}{Nk_B} - \frac{S_{cryst}(T^*)}{Nk_B}$$

$$= (C_{1ql} - C_{1cryst})\ln(T^*) + \left(\sum_{l=2}^{k}\left(\frac{l}{l-1}\right)C_{lql}\right.$$

$$\left. - \sum_{l=2}^{k}\left(\frac{l}{l-1}\right)C_{lcryst}\right)T^{*l-1}, \qquad (31)$$

where the subscript ql indicates the rapidly cooled liquid (and quenched glass). The second term on the right-hand-side corresponds to the anharmonicity ($\Delta S_{ah}/Nk_B$).

In Fig. 4(c), ΔS_{ah} was plotted as a function of T^*. ΔS_{ah} rapidly decreases with decreasing T^* and tends to converge to 0 at $T^* = 0$. A negative contribution to the anharmonic part of the entropy in a fcc crystal was previously found, while the contribution is smaller in a quenched glass.

A larger ΔS_{ah} is observed in the medium T^* region, where the non-equilibrium relaxation contributes. A steeper change in S for the quenched liquid corresponds to the change in U^* shown in Figs. 2(a) and 2(b).

The behavior of S at $T^* < T_g^*$ for the quenched glass is similar to that of the crystal because of the comparable slopes of the U^*/N versus T^* plots. This similarity is associated with the large contribution of the harmonic term for both cases, i.e., they have comparable C_1 values. This result explains the absence of the Kauzmann paradox.

Even if the entropy is comparable (note that we neglect the residual entropy for the glass at $T^* = 0$ in Eq. (31)), a difference between the glassy state and the crystal is clearly observed in the distributions of T_t^* or in their spectra.

J. Changes in the C_V obtained from the fluctuation along the *NVE* relaxation

Along with the slow *NVE* relaxation toward the glass branch, the C_V values that were obtained from the fluctuation of T_t^* and the distribution of T_t^* were examined, as shown in Figs. 5 and 6.
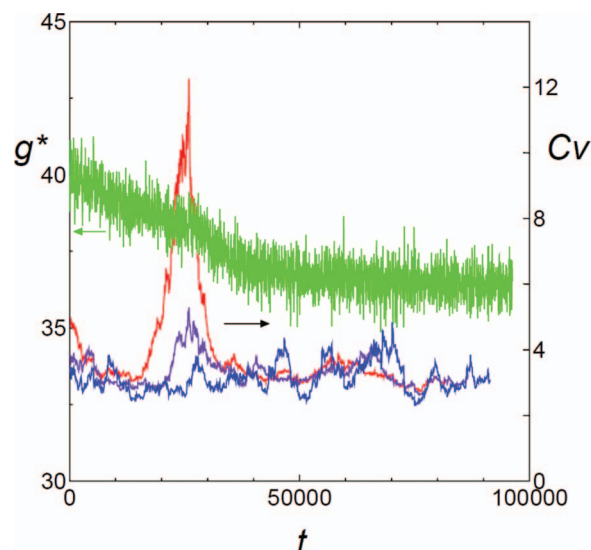

FIG. 5. Specific heat C_V obtained from the fluctuation of the kinetic energy by Eq. (30) along the *NVE* relaxation ($\rho_0^* = 1.48$) as a function of time. The values are calculated using three fixed averaging times. The data intervals used are 100 time steps (1 step = 1 fs for argon). Blue: the averaging of every 10 000 points. Purple: the averaging of every 20 000 points. Red: the averaging of every 30 000 points. The relaxation curve (light green) for g_t^* is shown in comparison. The curve of the time-dependent C_V shows a peak in the middle region, and its height depends on the averaging time.

In Fig. 5, the C_V values obtained from the fluctuation along the *NVE* relaxation using Eq. (30) are shown for $\rho_0^* = 1.48$ ($T_0^* = 0.21$) as a function of time.

The results for three fixed time windows, $\delta W = 10\,000$, 20 000, and 30 000 steps (1 step = 1 fs for argon), are shown by the blue, purple, and red curves, respectively. Here, data with an interval of 100 steps are used. At this T_0^*, non-equilibrium relaxation starts immediately after t_0 (see the relaxation curve of g^* (light green)); at this time, we start the observation under the *NVE* condition. The larger peak of C_V is found when a larger time window is used. A similar dependency on the time window was reported in Ref. 19. This result can be explained as follows. If the perturbation of the fluctuation that is caused by non-equilibrium relaxation is negligible, the peak is not clear, i.e., the peak height is enhanced if the longer time trend of the slope ($d < T_t^* > /dt$, where the averaging time is δW) overlaps the fluctuation of T_t^* during relaxation. If the beginning of the relaxation is included in the time span for the accumulation of the fluctuation, the value increases and then decreases. Thus, the observed C_V during *NVE* relaxation is affected by the slope of g^* (or U^*), and the low frequency mode (which corresponds to larger time windows) is more affected by the relaxation. In this case, the C_V has similar values before *NVE* relaxation and after it, but the latter value corresponds to metastable glass.

Both the large fluctuation before the relaxations and at the beginning of the relaxations can contribute to the maximum value of C_V, even in the rapidly quenched system.

The discrete character during *NVE* relaxation (the trapping in phase space) becomes clear when we examine the changes in the distribution of T_t^*. In Fig. 6(a), the changes in g_t^* and T_t^* during the run that starts at $T_0^* = 0.29$ ($\rho_0^* = 1.36$) are shown by the red and blue curves, respectively The
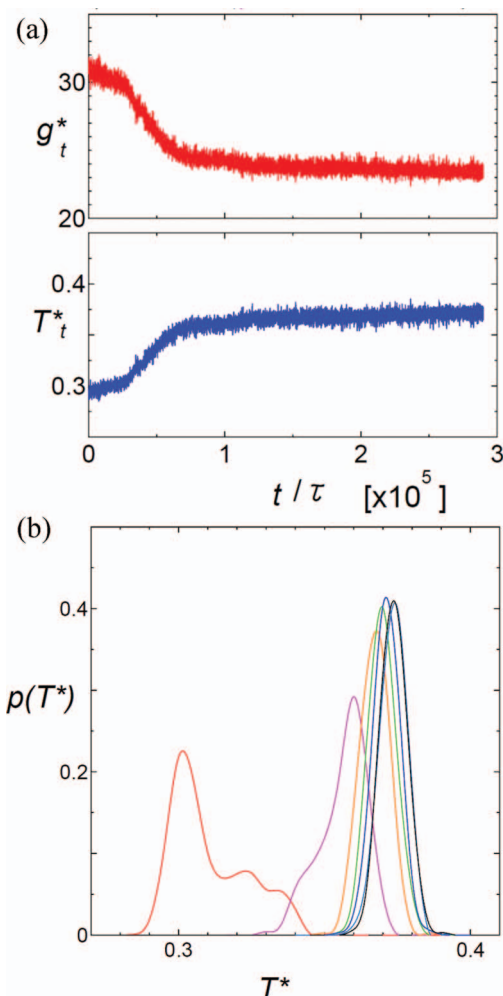
FIG. 6. (a) Changes in g* and in T^* along an *NVE* non-equilibrium relaxation during a 600 000-step run that starts from $\rho_0^* = 1.36$ and g* = 30.75. (b) Changes in the probability distribution of T_t^*, p(T^*), during the run. The distribution in each 100 000-step time region ($dt = 4.7 \times 10^4$) are shown from left to right. The distribution was normalized to 1 in each region. A change in the distribution occurs gradually but with discrete levels of states.
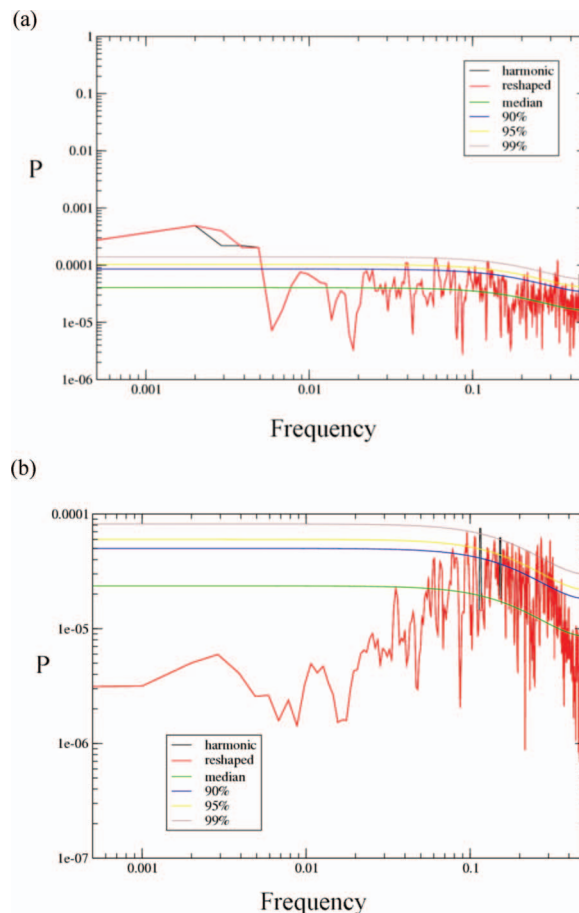

FIG. 7. Typical MTM spectra for (a) the liquid at $T^* = 0.52$ and (b) the crystal (fcc) at $T^* = 0.35$. Both spectra were obtained from the time series of T_t^* that is related to C_V for the run with 100 000 steps. In the reshaped spectrum (red), the contribution of harmonic signals (black) was removed.

observed time region was divided into six regions. In Fig. 6(b), the distributions of T_t^* at each 100 000-step (4.7×10^4) time region are shown from left to right for the same run. The distribution was normalized to 1 in each region. Several peaks or shoulders are found in each time region, and they gradually change with time.

When the system reaches the glass branch, the system does not show any further aging, at least during this specific time scale. Crystallization may occur toward the crystal branch over a longer time scale. Therefore, the Kauzmann paradox does not occur even in this case.

K. MTM spectra for liquid and supercooled-liquids

In Fig. 7, typical MTM spectra for a liquid at $T^* = 0.52$ and for a crystal (fcc) at $T^* = 0.35$ are shown. Both of these spectra were obtained from the time series of T_t^* for a 100 000-step run (100 ps for argon). A common time duration was used for the other MTM spectra. The Nyquist frequency,

$f_N = 0.5/dt$, is the highest frequency addressed, in which $dt = 0.1$ ps was used throughout this work.

At $T^* = 0.52$, in the liquid state, some harmonic components are found in the high frequency region, while a diffusive component appears at the lowest frequency.

Here, we examine the MTM spectra along *NVE* relaxation to determine what changes occur in the fluctuation of T^* in these regions. The MTM spectra of the time series of T_t^* with $T_0^* = 0.355(\geq T_P^*)$ exhibit a small power law region (a $1/f^\nu$ type dependence). Even in this region, harmonic oscillations contributed to the spectra (not shown). Before relaxation starts, the corresponding distribution of T^* is Gaussian-like, as confirmed by the Shapiro-Wilk (S-W) test.[31] We tested the data over the 100 000 steps using an interval of 100 steps against the null hypothesis that the data would be distributed normally. Based on the W (= 0.999) value in the S-W test, the null hypothesis was not rejected with a significance level of 1% ($P = 0.9105$), where $N = 1000$ (N is the number of samples) was used. Therefore, deviation from the Gaussian is not significant in this region.

The fluctuation of T^* increases with decreasing T^*. The MTM spectra were examined along the *NVE* relaxation. The spectra in the two time regions along the *NVE* relaxation are shown in Figs. 8(a) and 8(b) for $T^* = 0.29$ ($<T_P^*$). During
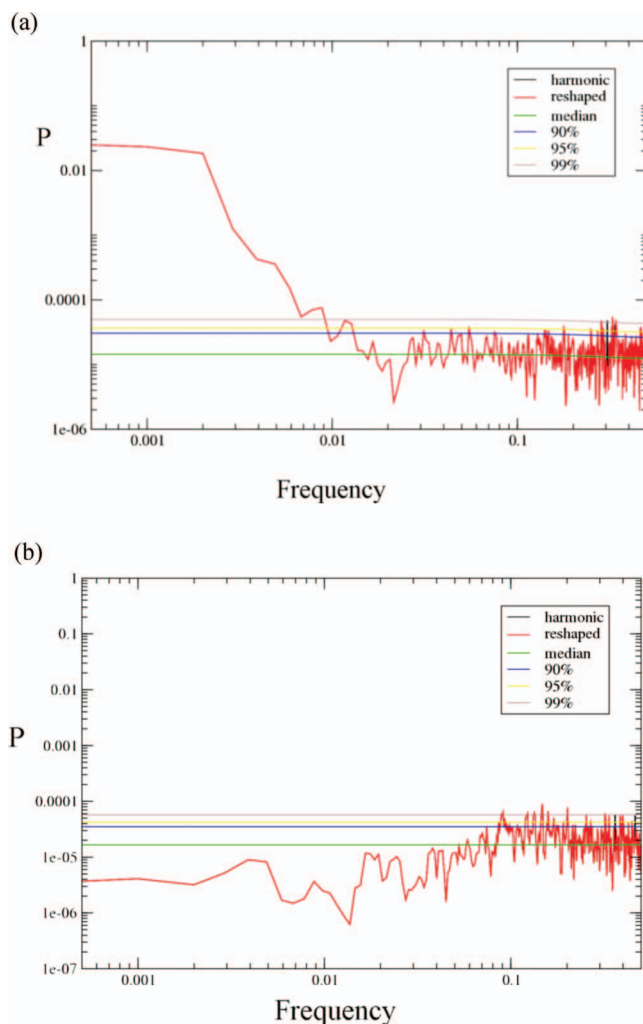
(a)

(b)

FIG. 8. MTM spectra for the time series of T_t^* during and after *NVE* relaxation. (a) $T_0^* = 0.355$ for the 100 000-step run after beginning relaxation. (b) After relaxation (500 000-600 000 steps) of the run in (a).

non-equilibrium relaxation, a power law behavior ($1/f^\nu$ type) is pronounced, and this behavior disappears when the system approaches the glass branch. For non-equilibrium relaxation, a long sampling time is required to obtain the mean behavior of the system due to the large contribution of the low-frequency mode. In the metastable state, the contribution of the low frequency part is small, similar to that in the crystal, while the broad distribution of the high-frequency region is similar to that in the liquid.

We previously examined the MTM spectra for the time series of the displacement of the heterogeneous one particle motion of lithium ions in a lithium metasilicate (Li_2SiO_3) glass.[32] The power law region that was observed in the spectra for T_t^* is similar to that in the MTM for the one particle motion of ions in an ionically conducting glass except for the collective character of the former. In the former, fluctuations or the intermittent changes in the distribution of T_t^* (or U_t^*) contribute, while, in the latter, the intermittent jump motions of the ions with heterogeneity (including back-correlated jumps and forward-correlated jumps) contribute.[33] For fast (diffusive) ions, the power law and high frequency (0.35–0.45) harmonic motions were found to be dominant, while, for slow

ions, broad peaks with harmonic motions were found mainly in the low frequency (0.03–0.14) region. In this case, the highest frequency, 0.5, corresponds to $1/2 \times 0.8$ (ps) in the real unit, i.e., the power law ($1/f^\nu$ type) spectrum of the time series of T^* corresponds to the power law region of the MSD and α-relaxation. The time scale that is required for the calculation of the thermodynamics will be significantly affected by the existence of the power law region.

V. CONCLUSION

We have examined the thermodynamic properties and the fluctuation of these properties in a single-component soft-core system along the phase diagram using the compressibility factor $\tilde{P}(T*)$ plotted against the reduced density ρ^* or the reduced temperature T^*. The specific heats C_V and C_P of the system can be represented by a function of $\tilde{P}(T^*)$ and by a function of the potential energy, U^*. Systems with a rapid quench that showed non-equilibrium *NVE* relaxation were examined. When the system was cooled to less than $T_P^* \sim 0.31$, the system fell out of equilibrium and was quickly trapped in a basin in the energy landscape. Even in the case of a rapid quench under other conditions, such as *NPT*, this type of relaxation should contribute to the changes in C_V to some extent.

For a longer time scale simulation (if the system was not quenched to the trapped states), the system reaches the glass branch, where the system is metastable. Once the system reaches the glass branch, further aging is not obvious within the observation time.

Several tendencies for the specific heat and entropy are found along with these processes as follows.

1. The specific heats, C_V, that are based on the fluctuation of T^* and on the derivative of the time-averaged energy coincide well with each other for both the equilibrated and quasi-equilibrated cases.
2. We applied an analytical expression of the entropy using polynomials to the quenched liquid (glass) in the soft-core model. The excess entropy (except for the residual entropy) can also be represented by the coefficients of polynomials. This result is useful in understanding the nature of the entropy term and its change in the phase diagram, including the problem of the Kauzmann paradox.
3. The origin of the maximum in C_V is the changes in the slope of g* (or U^*) due to the contribution of the non-equilibrium behavior of the system. The low frequency mode of T^* (and the related dynamics) is modified by non-equilibrium relaxation. An insufficient sampling of the phase space at $T^* < T_P^*$ also affects the thermodynamics.
4. A large peak in C_V was observed in both glass transition cases: one along the rapid quenching of the liquid and the other along the *NVE* relaxation. Therefore, thermodynamically, both processes along these paths are regarded as the glass transition.
5. The C_V values that are based on the fluctuations are sensitive to the time windows that are used for the

calculation. The value of C_V along the rapid quench is also affected by the non-equilibrium relaxation process that is related to the changes in the baseline of T^*, U^*, or g^*. The values of C_V will change in a discontinuous manner with a change in the derivative of g^* (or U^*) (see Eq. (9)) when narrow time and T^* windows are used for the observation, i.e., the changes in C_V (or C_P) at T_P^* and T_g^* are not necessarily continuous.

ACKNOWLEDGMENTS

[1] Y. Hiwatari, H. Matsuda, T. Ogawa, N. Ogita, and A. Ueda, Prog. Theor. Phys. **52**, 1105 (1974).

[2] M. Tanemura, Y. Hiwatari, H. Matsuda, T. Ogawa, N. Ogita, and A. Ueda, Prog. Theor. Phys. **58**, 1079 (1977); **59**, 323 (1978).

[3] M. Tanemura, H. Matsuda, T. Ogawa, N. Ogita, and A. Ueda, J. Non-Cryst. Solids **117/118**, 883 (1990)

[4] W. G. Hoover, M. Ross, K. W. Johnson, D. Henderson, J. A. Barker, and B. C. Brown, J. Chem. Phys. **52**, 4931 (1970); J. P. Hansen, Phys. Rev. A **2**, 221 (1970).

[5] J. Habasaki and A. Ueda, J. Chem. Phys. **134**, 084505 (2011).

[6] J. Habasaki and A. Ueda, Phys. Chem. Chem. Phys. **14**, 7120 (2012).

[7] W. Kauzmann, Chem. Rev. **43**, 219 (1948).

[8] J. C. Mauro, Int. J. Appl. Glass Sci. **2**, 245 (2011).

[9] The Multitaper Method (MTM) provides a useful spectral estimation in the nonparametric manner. A set of independent estimates of the power spectrum is computed by pre-multiplying the data by orthogonal tapers, which are constructed to minimize the spectral leakage due to the finite length of the dataset. Estimation using a single window corresponds to the special case with a single taper. The method can be used for a reconstruction of time series, which are containing both continuous and singular components (see Refs. 10 and 11 for details).

[10] M. E. Mann and J. M. Lees, Clim. Change **33**, 409–445 (1996).

[11] D. B. Percival and A. T. Walden, *Spectral Analysis for Physical Applications–Multitaper and Conventional Univariate Techniques* (Cambridge University, 1993).

[12] H. Ogura, H. Matsuda, T. Ogawa, N. Ogita, and A. Ueda, Prog. Theor. Phys. **58**, 419 (1977).

[13] T. L. Hill, *An Introduction to Statistical Thermodynamics* (Addison-Wesley Pub. Comp., 1960).

[14] J. H. R. Clarke, J. Chem. Soc., Faraday Trans. 2 **75**, 1371 (1979).

[15] J. N. Cape and L. V. Woodcock, J. Chem. Phys. **72**, 976 (1980).

[16] O. Yamamuro, I. Tsukushi, A. Lindqvist, S. Takahara, M. Ishikawa, and T. J. Matsuo, J. Phys. Chem. B **102**, 1605 (1998).

[17] N. C. Forero-Martinez, R. Cortes-Huerto, and P. Ballone, J. Chem. Phys. **136**, 204510 (2012).

[18] J. C. Mauro, R. J. Loucks, and S. Sen, J. Chem. Phys. **133**, 164503 (2010).

[19] J. L. Lebowitz, J. K. Percus, and L. Verlet, Phys. Rev. **153**, 250 (1967).

[20] H. M. Carruzzo and C. C. Yu, Phys. Rev. E **66**, 021204 (2002).

[21] C. C. Yu and H. M. Carruzzo, Phys. Rev. E **69**, 051201 (2004).

[22] D. N. Perera and P. Horrowell, Phys. Rev. E **59**, 5721 (1999).

[23] F. G. Padilla, P. Harrowell, and H. Fynewever, J. Non-Cryst. Solids **307–310**, 436 (2002).

[24] T. Tao, T. Odagaki, and A. Yoshimori, J. Chem. Phys. **122**, 044505 (2005).

[25] D. Kivelson and G. Tarjus, J. Chem. Phys. **109**, 5481 (1998).

[26] C. A. Angell and C. Tucker, J. Phys. Chem. **78**, 278 (1974).

[27] J. H. Gibbs and E. A. DiMarzio, J. Chem. Phys. **28**, 373 (1958).

[28] F. H. Stillinger, J. Chem. Phys. **88**, 7818 (1988).

[29] R. J. Speedy, Biophys. Chem. **105**, 411 (2003).

[30] J. M. Gordon, J. H. Gibbs, and F. D. Fleming, J. Chem. Phys. **65**, 2771 (1976).

[31] S. Shapiro and M. Wilk, Biometrica **52**, 591 (1965).

[32] J. Habasaki, K. L. Ngai, and Y. Hiwatari, J. Chem. Phys. **122**, 054507 (2005).

[33] J. Habasaki and K. L. Ngai, J. Chem. Phys. **129**, 194501 (2008).